Immobilization of Selenite via Two Parallel Pathways during *In-situ* Bioremediation

Youneng Tang[*, §, **], Charles J. Werth[*, †], Robert A. Sanford[‡], Rajveer Singh[*], Kyle Michelson[*], Masaru Nobu[*], Wen-Tso Liu[*], Albert J. Valocchi[*]

* Department of Civil and Environmental Engineering, University of Illinois at Urbana-Champaign

† Department of Civil, Architectural, and Environmental Engineering, University of Texas at Austin

‡ Department of Geology, University of Illinois at Urbana-Champaign

§ Department of Civil and Environmental Engineering, FAMU-FSU College of Engineering, Florida State University

** Corresponding author: 2525 Pottsdamer Street, Building A, Suite A130 Tallahassee, FL 32310; (850)4106119; ytang2@fsu.edu

ABSTRACT

It is widely understood that selenite can be biologically reduced to elemental selenium. Limited studies have shown that selenite can also be immobilized through abiotic precipitation with sulfide, a product of biological sulfate reduction. We demonstrate that both pathways significantly contribute to selenite immobilization in a microfluidic flow cell having a transverse mixing zone between propionate and selenite that mimics the reaction zone along the margins of a selenite plume undergoing bioremediation in the presence of background sulfate. The experiment showed that red particles of amorphous elemental selenium precipitate on the selenite-rich side of the mixing zone, while long crystals of selenium sulfides precipitate on the propionate-rich side of the mixing zone. We developed a continuum-scale reactive transport model that includes both pathways. The simulated results are consistent with the experimental results, and indicate that spatial segregation of the two selenium precipitates is due to the segregation of the more thermodynamic favorable selenite reduction and the less thermodynamically favorable sulfate reduction. The improved understanding of selenite immobilization and the improved model can help to better design *in-situ* bioremediation processes for groundwater contaminated by selenite or other contaminants (e.g., uranium (IV)) that can be immobilized via similar pathways.

Table of contents art

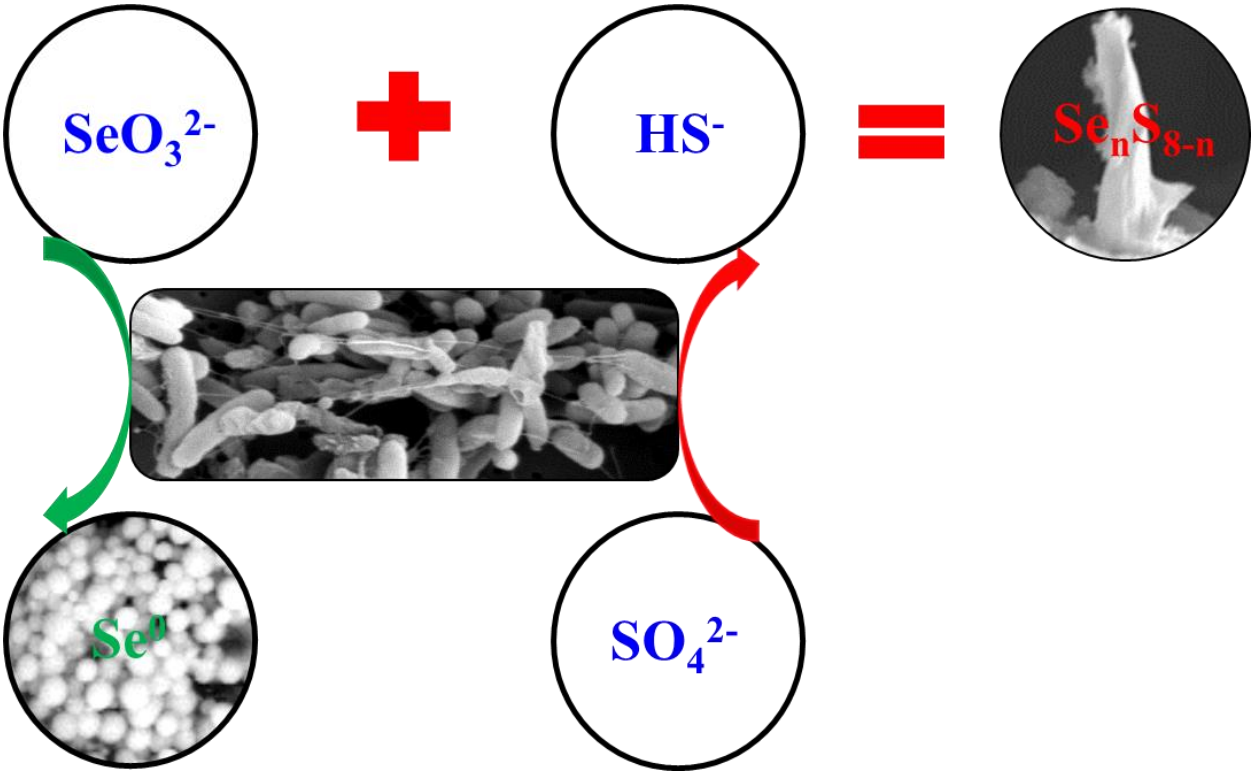

KEYWORDS:

Abiotic selenite immobilization; biotic selenite immobilization; microfluidic flow cell; reactive transport model; selenium sulfide

INTRODUCTION

Selenium is an essential element for humans and animals but is very toxic at high concentrations. A broad spectrum of anthropogenic activities, including mining, agricultural, petrochemical, and industrial manufacturing operations, can cause selenium contamination in the environment,[1] including the contamination of groundwater.[26] Selenium ranks 145 among a list, in order of priority, of 275 substances that are commonly found at facilities on the National Priorities List.[25] The typical concentration of selenium in groundwater ranges from 0.06 - 400 µg /L, but concentrations may approach 6000 µg /L.[26] High concentration of selenium causes human health problems such as hair or fingernail loss, numbness in fingers or toes, and circulatory problems.[2] The U.S. Environmental Protection Agency established a maximum contaminant level for total selenium in drinking water at 50 µg /L.[2] Higher-than-required concentration of selenium also causes health problems for livestock and wildlife. One example is mortality, birth defects, and reproductive failure in waterfowl at Kesterson National Wildlife Refuge, San Joaquin Valley, California.[35] These problems were attributed to elevated concentrations of selenium in irrigation drainage that discharged to the refuge.

Selenium predominantly occurs in the form of selenate (SeO_4^{2-}, Se(VI)), selenite (SeO_3^{2-}, Se(IV)), elemental selenium (Se^0, Se(0)), and selenide (Se^{2-}). The dominant forms of selenium in groundwater are oxidized selenium, i.e., selenate and selenite, and groundwater contaminated by these contaminants can be bioremediated by injecting an electron donor into the contaminated

zone, where Se-respiring bacteria reduce the oxidized selenium to immobile elemental selenium by coupling this reaction to the oxidation of the added electron donor.[3-7] A growing body of literature indicates that amended electron donors mix with contaminants in groundwater plumes via transverse diffusion along plume margins.[11-13] Although transverse mixing affects the spatial distribution and time scales of product formation (e.g., elemental selenium), as well as the influence of other reactive species present in groundwater, prior work has not evaluated the influence of diffusive mixing on selenium bioremediation. Se-respiring microorganisms are similar to dissimilatory metal-reducing bacteria (DMRB; e.g. iron reducing bacteria) since they reduce some metals in environments like groundwater to an insoluble state, such as U(VI) reduction to U(IV) and Cr(VI) reduction to Cr(III).[5] Insights into selenium immobilization via biostimulation have the potential to impact how the bioremediation of other metal contaminated sites are evaluated.

In this study, we use selenite as the contaminant for two reasons. First, selenite is an intermediate of selenate reduction. Using selenite simplifies the system and allows more direct mechanistic interpretation of the results. Second, most previous studies used selenite instead of selenate (probably due to the first reason); thus, a complete set of parameters are available in the literature for modeling selenite. More than 20 bacterial species have demonstrated capability to respire selenite.[33] Potential mechanisms and enzyme systems involved in biological selenite transformations have been proposed for some of the selenite-respiring species, such as

Rhodospirillum rubrum, *Rhodobacter capsulatus*, *Geobacter sulfurreducens*, *Shewanella oneidensi and Veillonella atypica*.[1, 6, 34] Though selenide and methylated forms of selenium may be produced, elemental selenium nanoparticles are the main product.[35] The structural and spectral features of the selenium nanoparticles have been characterized.[4]

Sulfate is a common co-constituent in groundwater with selenite, and its reduction to sulfide leads to another pathway to immobilize and reduce selenite. Previous studies of the abiotic reaction between sulfide and selenite have found that precipitation of solid phase selenium sulfides depends on the pH of the solution, occurring at between pH 3 and 10. At pH<3 or pH>10, the reaction yields a mixture of elemental sulfur and elemental selenium.[8, 9] The reaction kinetics of this abiotic reaction has been well studied and quantified.[9] However, there is only one study where biological reduction of sulfate was coupled to abiotic selenite reduction with sulfide; Hockin and Gadd[10] used a strain of *Desulfomicrobium novegicum* to reduce sulfate to sulfide, which then abioticaly reacted with selenite in a glass vial. No previous research has investigated this reaction in the context of reactive transport conditions.

At a bioremediation site with groundwater at circumneutral pH, we expect that some selenite would be reduced to elemental selenium via selenite-reducing bacteria (SeRB), or converted to selenium sulfides via the abiotic reaction that is mediated by sulfate-reducing bacteria (SRB). However, simultaneous immobilization of selenite via the two pathways has not been studied, to

the best of our knowledge. Therefore, the first objective of this study is to determine if the two pathways simultaneously occur and to what extent might each pathway contribute to selenite immobilization during bioremediation.

Concentration gradients of the electron donor and acceptor during transverse diffusion at the margins of groundwater plumes can be steep, which may lead to uneven distribution of reaction products, namely different microbial species, elemental selenium, and selenium sulfides. Therefore, the second objective of this study is to investigate typical distribution patterns of the reaction products in the mixing zone by integrating experiment with modeling. In previous reactive transport models for *in-situ* bioremediation of selenite-contaminated groundwater, the abiotic, but biologically mediated selenite removal pathway was neglected due to inadequate understanding of this pathway.[14, 15] We improve the model by adding this pathway, and use the improved model to more accurately predict selenite immobilization performance and the typical distribution patterns of the reaction products.

MATERIALS AND METHODS

Micro-fluidic Flow Cell Experiment

Flow cell description

A microfluidic flow cell experiment was conducted to mimic the mixing zone in a site heavily contaminated by selenite. Figure 1a shows the set-up of the flow cell. The dimensions of the flow cell were 2 cm (length) × 1 cm (width) × 20 μm (height). The flow cell contained a homogeneous pore network that consisted of a uniform distribution of 300-μm-diameter cylindrical posts (Figure 1b). Each pore body was 180 μm and each pore throat was 40 μm; this resulted in a porosity of 0.39. The flow cell was fabricated through a standard photolithography procedure as described in our previous work, e.g., Chomsurin and Werth,[36] Willingham et al.[16] and Zhang et al.[13] A silicon wafer was coated with a photoresist (PR) polymer, and selectively exposed to UV light by placing a mask directly above the wafer. The areas exposed to UV light were weakened, and were removed using a developer. Exposed areas of silicon were etched using plasma generated from an inductively coupled plasma-deep reactive ion etching system. Then flow channels were formed by anodically bonding thin Pyrex glass to the top of the etched silicon wafer.

Control experiment without biomass

To determine if any chemical reactions would occur without biomass in the flow cell, the flow cell was operated at the following conditions in a 30 ^{0}C room for one month. Mineral salts

solution containing selenite (5 mol/m^3) was supplied at inlet A, and mineral salts solution containing propionate (10 mol/m^3) was supplied at inlet B (Figure 1a). The flow rates at both inlets were maintained at the same rate using a syringe pump (Cole Parmer, 74900 series), connected to the flow cell with 1/16"-diameter PEEK^{TM} tubing. The flow rate corresponded to a Darcy velocity of 8.4 m/day. Sulfate was present in the mineral salts solution at 0.1 mol/m^3. The mineral salts solution (per liter of deionized water) contained: $FeSO_4$ •$7H_2O$, 0.007 g; Na_2SO_4, 0.005 g; $CaCl_2$•$2H_2O$, 0.015 g; $MgCl_2$•$6H_2O$, 0.02 g/L; NH_4Cl, 0.1 g/L, and trace elements that included $MnCl_2$•$4H_2O$ (5 mg/L), H_3BO_3 (0.5 mg/L), $ZnCl_2$ (0.5 mg/L), $CoCl_2$•$6H_2O$ (0.5 mg/L), $NiSO_4$•$6H_2O$ (0.5 mg/L), $CuCl_2$•$2H_2O$ (0.3 mg/L), $NaMoO_4$•$2H_2O$ (0.1 mg/L), Na_2SeO_4 (0.003 mg/L) and Na_2WO_4 (0.008 mg/L). KH_2PO_4 (2 mM) and $NaHCO_3$ (10 mM) were added as pH buffers. The solution was degased using N_2 + CO_2 gas while maintaining pH at ~7.0. Na_2SO_3 (0.04 mM) was added to the solution to consume the residual dissolved oxygen. The mineral salts solution was autoclaved. Since no precipitation occurred during the control experiment, we inoculated the flow with biomass, as discussed in the next section.

Inoculation

After the control experiment was completed, the flow cell was inoculated with a mixed culture enriched from a groundwater sample taken from the Oak Ridge superfund site in East Tennessee. Before inoculation, we confirmed that the mixed culture could reduce selenite and sulfate in

sealed serum bottles. For inoculation, mineral salts solution that contained the mixed culture, propionate, and fumarate were delivered to both inlets and flowed through the flow cell for three weeks at a Darcy velocity of 1.2 m/day. At the end of the inoculation period, small areas with biomass growth were observed to develop randomly but uniformly in the flow cell, as shown in Supporting Information (Figure S1).

Operation and imaging

After the inoculation, the flow cell was operated using the same conditions as in the control experiment for 40 days. The flow cell was imaged weekly by a Nikon Epiphot 200 epi-fluorescent microscope with a 20 × objective and a RT Spot charge-coupled device (CCD) digital camera; this was also done weekly for the control experiment and the inoculation and enrichment. To characterize the reaction products, we filtered the effluent of the flow cell by a membrane that had a maximum pore size of 0.2 μm on the 36th day, and then assayed the retentate on the membrane using a Field-Emission Environmental Scanning Electron Microscope (Philips XL30 ESEM-FEG) with Energy-Dispersive Spectroscopy (EDS). To further characterize the reaction products in the flow cell, color images of the flow cell were taken on the 40th day using a Leica microscope with a 40 × objective and a CCD camera (Qimaging Retiga 2000R Fast 1394), and Raman spectra of the reaction products were obtained the next day using a high-resolution research-grade Horiba LabRAM HR 3D-capable Raman spectroscopy imaging system with an excitation wavelength of 523 nm. Then the flow cell was cut into 2

mm-wide pieces along the direction perpendicular to flow using a Disco DAD-6TM Wafer Dicing Saw. The cut pieces were fixed, dehydrated, and coated with Au/Pt before being assayed by the same ESEM-EDS system as above.

Reactive Transport Modeling

Model overview

To interpret the experimental observations, we developed a reactive transport model. The model was based on the widely used continuum-scale reactive transport model framework, but modified to include the unique metabolic and physiological characteristics of sulfate and selenite reducing bacteria. Although pore-scale models have been developed for coupled flow, transport, reaction, and biofilm growth,[17-19] we adopt a simpler continuum-scale model since our goal is to understand (not directly replicate) the effects of mixing on spatial segregation of the two different reaction pathways. Five major reactions are considered in our model and they are listed below. Reactions 1 and 2 are mediated by SRB and Reactions 3 and 4 are mediated by SeRB.[20] Reaction 5 is an abiotic reaction for selenite and sulfide.[9] Therefore, the model considers two biomass species (SRB and SeRB), five dissolved chemical species ($CH_3CH_2COO^-$, SeO_3^{2-}, SO_4^{2-}, HS^-, and CH_3COO^-), and two solid chemical species (Se_nS_{8-n}, Se^0).

$$CH_3CH_2COO^- + 0.75SO_4^{2-} \rightarrow CH_3COO^- + HCO_3^- + 0.75HS^- + 0.25H^+ \quad (1)$$

$$CH_3COO^- + SO_4^{2-} \rightarrow 2HCO_3^- + HS^- \quad (2)$$

$$CH_3CH_2COO^- + 1.5SeO_3^{2-} + 2H^+ \rightarrow CH_3COO^- + HCO_3^- + 1.5Se^0 + 1.5H_2O \quad (3)$$

$$CH_3COO^- + 2SeO_3^{2-} + 3H^+ \rightarrow 2HCO_3^- + 2Se^0 + 2H_2O \quad (4)$$

$$SeO_3^{2-} + 2HS^- + 4H^+ \rightarrow (3/8)Se_{8/3}S_{16/3} + 3H_2O \quad (5)$$

For simplification, the total concentration of a dissolved chemical species (e.g., the sum of SeO_3^{2-}, $HSeO_3^-$, and H_2SeO_3) is denoted by the concentration of the dominant species (i.e., SeO_3^{2-}) at pH 7.2, which is the pH value measured at the effluent of the flow cell; the total concentration of selenium sulfides, Se-S solids consisting of the ring molecules Se_nS_{6-n}, Se_nS_{7-n}, and Se_nS_{8-n},[21] is denoted by the concentration of the dominant species (i.e., Se_nS_{8-n}) identified by Geoffroy and Demopoulos[8]. We use fixed stoichiometric coefficients in Se_nS_{8-n}, and denote this solid as $Se_{8/3}S_{16/3}$ in reaction 5. This represents an average composition of Se_nS_{8-n} molecules, and the ratio of Se to S is consistent with the composition of the selenium sulfides produced in Geoffroy and Demopoulos[8].

Governing equations

The model consists of mass balance equations for five dissolved chemical species, denoted as $C_{D,i}$ (i = 1-5), two solid chemical species, denoted $C_{s,m}$ (m = 1-2), and two biomass species, denoted $C_{x,n}$ (n = 1-2). These species participate in reactions 1 through 5 (j = 1-5) given above. Full details are given in the Supporting Information (Table S1). Reactive transport of the five dissolved chemical species is simulated using the continuum-scale advection-dispersion-reaction equation:

$$\frac{\partial}{\partial t}(\phi C_{D,i}) = D_T \frac{\partial^2 C_{D,i}}{\partial y^2} - U \frac{\partial C_{D,i}}{\partial x} + R_{D,i} \qquad 6$$

The overall reaction rate $R_{D,i}$ for dissolved species i is a function of the rates of reactions 1 through 5, as shown in Table S1. Longitudinal dispersion is neglected in the equation since advection dominates over dispersion along the flow direction due to the short travel time in the microfluidic flow cell.[12] All parameters used in this paper are defined in Tables 1 (Model inputs) and 2 (Model outputs). We use reasonable parameters from the literature for similar conditions. The reaction terms for all chemical species and biomass species are summarized in the Supporting Information (Table S1). Biomass growth is simulated using the growth-decay equation:[22]

$$\frac{dC_{X,n}}{dt} = R_{X,n} - bC_{X,n} \qquad 7$$

Precipitation of selenium sulfides (reaction 5) is described by the second order kinetics in Pettine et al.[9] and precipitation of elemental selenium is stoichiometrically related to biological selenite reduction (reactions 3 and 4):

$$\frac{dC_{S,m}}{dt} = R_{S,m} \qquad 8$$

Initial conditions, boundary conditions, and numerical solution methods

The initial conditions, boundary conditions, and numerical solution methods are similar to those in our previous work that simulated the microbial mediated reactive transport in microfluidic flow cells.[17, 19] We modify them slightly by adding the numerical solution for the solid chemical species and present the modified version in Supporting Information.

RESULTS AND DISCUSSIONS

Segregation of Two Solid Chemical Species

Figure 2 shows images of the flow cell on the 1st, 20th, and 40th days after inoculation and enrichment. Reaction products accumulated gradually in the mixing zone of the flow cell. To obtain the pore-scale morphology of the reaction products, a representative part of the mixing zone (downstream) in Figure 2a-c is magnified in Figure 2d-f. To avoid the impacts of small fluctuations of inflow caused by the AC (alternating current)-powered syringe pump near the inlet, we did not evaluate the mixing zone in this part of the micromodel. The fluctuation

caused the mixing zone to move up and down in this area, and this smeared the distribution pattern of reaction products. Instead, we focused on the mixing zone close to the outlet, where the flow was fully developed and fluctuations were dampened. A similar phenomenon was observed in our previous studies with microfluidic flow cells.[13, 27]

To distinguish the reaction products, a color image of the representative part of the mixing zone was taken on the 40th day (Figure 3). Two solid chemical species were produced and segregated in the mixing zone. One was red spherical particles of diameters 2 μm or less. They were dominant on the selenite-rich side, and they aggregated to form "bridges" connecting cylindrical posts and oriented in the flow direction. The morphology of these bridges seems to overlap the biofilm morphology reported in other similar micro-fluidic flow cell experiments.[13] Bacteria stay in the bridge-shaped areas since the shear stress is smaller there.[19] The overlap between biofilms and red particles suggests that these particles may be produced directly from biological activity. The other type of precipitate was 10-50 μm long crystals (Figure 3). They were dominant on the propionate-rich side and were randomly distributed in pore throats and bodies. Another representative section of the mixing zone from the same experiment (the end of the mixing zone, shown in Figure S4) shows a similar distribution pattern.

Characterization of the Two Solid Chemical Species

To characterize any products being created in the system, we filtered the effluent through a membrane on the 36th day and assayed the retentate on the membrane using ESEM. We observed small elemental selenium particles attached to bacterial appendages and surfaces (Figure 4). The composition of the particles was confirmed by EDS tests (data not shown). Selenium particles of similar size were reported in other studies of biological selenite reduction.[1, 4, 6] The attachment of selenium particles to biomass further indicates that the particles are closely linked to biological activity. No long crystals appeared in the effluent despite their clear formation within the flow cell.

To further characterize the reaction products, we obtained Raman spectra of more than 50 locations in the mixing zone. Spectra corresponding to the three representative locations are shown in Figure 5. Figure 5a shows the spectrum for the red particles (Position 1 in Figure 3b). It has only two peaks: one (262.5 cm^{-1}) for amorphous elemental selenium and the other (523.1 cm^{-1}) corresponding to silicon, the main elemental composition of the flow cell.[23] Figure 5b shows the spectrum for the long crystals (Position 2 in Figure 3c); all the peaks correspond to selenium sulfides except the expected peak for silicon: 84.6, 155.4, 222.0, and 473.0 cm^{-1} correspond to the S-S bonds; 357.5 cm^{-1} corresponds to the Se-S bonds in the structure unit -S-Se_n-S- ($n \geq 2$); 379.2 cm^{-1} corresponds to the Se-S bonds in the structure unit –S-Se-S-; 262.5 cm^{-1} corresponds to the Se-Se bonds.[21, 23] Figure 5c shows the spectrum for a bridge-shaped

aggregate (Position 3 in Figure 3b); this spectrum has all the peaks in Figures 5a and 5b, but the highest and biggest peak is 262.5 cm^{-1}, suggesting the bridge-shaped aggregate is dominated by amorphous elemental selenium with small amounts of selenium sulfides. The Raman spectra suggest two pathways of selenite immobilization: one is elemental selenium formation through biological selenite reduction and the other is precipitation of selenium sulfides due to abiotic reaction between selenite and sulfide, a biological product of sulfate reduction.

To confirm the composition of the two solid chemical species in the flow cell we cut the flow cell across the porous network so that the mineral precipitates could be directly observed in a vertical cross section without obstruction from glass or silicon. The two types of chemical precipitates were observed using ESEM, and their composition was determined using EDS. Representative images of the two chemical solid species are shown in Figures 6a and 6b, respectively. The EDS spectra of the two species are shown in Figure S2. While the red particles only contained selenium, the long crystals contained selenium and sulfur at an atomic ratio of ~0.55. This ratio is close to the stoichiometric ratio of SeO_3^{2-}/HS^- in Reaction 5 (0.5).

Explanation for the Segregation of the Two Solid Species

The reactive transport model was used to simulate the distribution of the two solid chemical species. The results shown in Figure 7 are consistent with the experiment in terms of the relative locations of the two solid chemical species. Elemental selenium and selenium sulfides

precipitate in the mixing zone, with selenium sulfides distributed towards the bottom side (i.e., propionate-rich side) and elemental selenium towards the top side (i.e., selenite-rich side). The segregation of solid chemical species is due to the spatial distribution of different bacterial activities affiliated with different populations that lead to the generation of each type of selenium precipitate observed (Figure 7): The selenite reducing bacteria (SeRB) growth zone overlaps the elemental selenium precipitation zone, and the zone that has the highest concentration of selenium sulfides contains populations of sulfate reducing bacteria (SRB). Two factors may explain why most SRB grow on the propionate-rich side of the mixing zone. First, the oxidation of propionate produces acetate (Reactions 1 and 3), which accumulates along the centerline in the mixing zone (Figure S3d); this electron donor and carbon source promotes the growth of SRB, which explains why SRB have the highest concentration in the mixing zone. Second, SeRB outcompete SRB for the same electron donors (propionate and acetate) because selenite reduction yields more energy and more growth as indicated by the reduction reaction thermodynamics shown in Equations 9 and 10;[24] this explains why the concentration of SRB is higher on the propionate-rich side than on the selenite-rich side.

$$\frac{1}{8}SO_4^{2-} + \frac{9}{8}H^+ + e^- \rightarrow \frac{1}{8}HS^- + \frac{1}{2}H_2O, \quad \Delta G = -24.0\ kJ/mol \qquad 9$$

$$\frac{1}{4}SeO_3^{2-} + \frac{3}{2}H^+ + e^- \rightarrow \frac{1}{4}Se^0 + \frac{3}{4}H_2O, \quad \Delta G = -87.1\ kJ/mol \qquad 10$$

The difference in thermodynamics is considered in the model by using higher biomass yield coefficients for SeRB than for SRB (Table 1).

While the relative locations of the two chemical species in the mixing zone are consistent between the experiment and the model, the absolute locations of the mixing zones are different. In the model, the mixing zone is essentially symmetric about the centerline, but in the experiment, the mixing zone curves towards the selenite-rich side. The difference may be explained by a simplification in the model. In the experiment, selenium sulfides are long crystals and they tend to precipitate towards the bottom side (i.e., propionate-rich side), which slightly pushes the flow and the mixing zone towards the top side (i.e., selenite-rich side) in the experiment. However, this flow direction change due to precipitation is not considered in the model.

Implications of this Study

This study shows that selenite can be simultaneously immobilized through two pathways during *in-situ* bioremediation. One is biological reduction to elemental selenium, and the other is precipitation with sulfide that is produced by SRB. In our study, both pathways significantly contributed to selenite immobilization, as shown in Figures 3 (experimental results) and 7 (simulated results). We anticipate that the contribution of each pathway would depend on conditions such as concentrations of selenite, sulfate, and injected electron donor, the flow rate,

and the characteristics of the porous media in a system. We do not quantify the contribution of the two pathways in our study since we only have one set of experimental data, which are not enough to support parameter optimization. This could be quantified in future research by investigating selenite immobilization under a range of conditions, and could be systematically studied by using reactive transport models with optimized parameters. Understanding the contribution of each pathway is fundamental to designing *in-situ* bioremediation processes, and incorporating both pathways into reactive transport models can increase the accuracy of model prediction.

ACKNOWLEDGEMENT

This paper is supported by the U.S. Department of Energy under Award No. DE-SC0006771 to the University of Illinois at Urbana-Champaign. Disclaimer: This paper was prepared as an account of work sponsored by an agency of the United States Government. Neither the United States Government nor any agency, thereof, nor any of their employees, makes any warranty, express or implied, or assumes any legal liability or responsibility for the accuracy, completeness, or usefulness of any information, apparatus, product, or process disclosed, or represents that its use would not infringe privately owned rights. The views and opinions of authors expressed herein do not necessarily state or reflect those of the United States Government or any agency thereof.

SUPPORTING INFORMATION AVAILABLE

The supporting information contains one table to summarize the reaction, species, and rate matrix used in the model, one section to explain the initial conditions, boundary conditions, and numerical solutions for the model, one figure to show the distribution of dissolved chemical species in the model, and three figures to characterize the solid reaction products in the experiment. This information is available free of charge via the Internet at http://pubs.acs.org/ .

REFERENCES

(1) Pearce, C. I.; Pattrick, R. A.; Law, N.; Charnock, J. M.; Coker, V. S.; Fellowes, J. W.; Oremland, R. S.; Lloyd, J. R. Investigating different mechanisms for biogenic selenite transformations: *Geobacter sulfurreducens, Shewanella oneidensis* and *Veillonella atypical*. *Environ. Technol.* **2009**, 30(12), 1313-1326.

(2) U.S. Environmetal Protection Agency. National primary drinking water standard. EPA 816-F-03-016, Office of groundwater and drinking water (4606M): Washington, DC, **2003**.

(3) Oremland, R. S.; Hollibaugh, J. T.; Maest, A. S.; Presser, T. S.; Miller, L. G.; Culbertson, C. W. Selenate reduction to elemental selenium by anaerobic bacteria in sediments and culture: biogeochemical significance of a novel, sulfate-independent respiration. *App. Environ. Microbiol.* **1989**, 55(9), 2333-2343.

(4) Oremland, R. S.; Herbel, M. J.; Blum, J. S.; Langley, S.; Beveridge, T. J.; Ajayan, P. M.; Sutto, T.; Ellis, A. V.; Curran, S. Structural and spectral features of selenium nanospheres produced by se-respiring bacteria. *App. Environ. Microbiol.* **2004**, 70(1), 52-60.

(5) Lovley, D. R. 1995. Bioremediation of organic and metal contaminants with dissimilatory metal reduction. *J. Ind. Microbiol.* **1995**, 14, 85-93.

(6) Kessi, J.; Ramuz, M.; Wehrli, E.; Spycher, M.; Bachofen, R. Reduction of selenite and detoxification of elemental selenium by the phototrophic bacterium *Rhodospirillum rubrum*. *App. Environ. Microbiol.* **1999**, 65(11), 4734-4740.

(7) Klonowska, A.; Heulin, T.; Vermeglio, A. Selenite and tellurite reduction by *Shewanella oneidensis*. *App. Environ. Microbiol.* **2005**, 71(9), 5607-5609.

(8) Geoffroy N.; Demopoulos, G. P. The elimination of selenium (IV) from aqueous solution by precipitation with sodium sulfide. *J. Hazard. Mater.* **2011**, 185, 148-154.

(9) Pettine, M.; Gennari, F.; Campanella, L.; Casentini, B.; Marani, D. The reduction of selenium (IV) by hydrogen sulfide in aqueous solutions. *Geochim. Cosmochim. Ac.* **2012**, 83, 37-47.

(10) Hockin, S. L.; Gadd, G. M. linked redox precipitation of sulfur and selenium under anaerobic conditions by sulfate-reducing bacterial biofilms. *Appl. Environ. Microbiol*. **2003**, 69(12), 7063-7072.

(11) Zhou Q. X.; Song Y. F. *Contaminated Soil Remediation: Principles and Methods (in Chinese)*; Science Press: Beijing, China, **2004**.

(12) Cirpka, O.; Valocchi, A. J. Two-dimensional concentration distribution for mixing-controlled bioreactive transport in steady state, *Adv. Water Resour.* **2007**, 30(6/7), 1668-1679.

(13) Zhang, C.; Kang, Q.; Wang, X.; Zilles, J. L.; Müller, R. H.; Werth, C. J. Effects of pore-scale heterogeneity and transverse mixing on bacterial growth in porous media, *Environ. Sci. Technol*. **2010**, 44, 3085-3092.

(14) Tayfur, G.; Tanji, K. K.; Baba, A. Two-dimensional finite elements model for selenium transport in saturated and unsaturated zones. *Environ. Monit. Assess.* **2010**, 169: 509-518.

(15) Rajabli, J. N.; Mirbagheri, S. A.; Hasani, A. H.; Javid, A. H. Two-dimensional finite differences model for selenium transport and transformation in soil column and ground water contamination prediction (Case study: Gonbad-e Kavous site). *Eur. J. Exp. Biol*. **2013**, 3(3): 291-300.

(16) Willingham, T. W.; Werth, C. J.; Valocchi, A. J. Evaluation of the effects of porous media structure on mixing-controlled reactions using pore-scale modeling and micromodel experiments. *Environ. Sci. Technol.* **2008**, 42(9), 3185-3193.

(17) Knutson, C. E.; Werth, C. J.; Valocchi, A. J. Pore-scale simulation of biomass growth along

the transverse mixing zone of a model two-dimensional porous medium, *Water Resour. Res.* **2005**, 41, W07007, doi:10.1029/2004WR003459.

(18) Tartakovsky, A. M., Scheibe, T. D.; Meakin, P. Pore-scale model for reactive transport and biomass growth. *J. Porous Media* **2009**, 12(5), 417-434.

(19) Tang, Y.; Valocchi, A. J.; Werth, C. J.; Liu, H. An improved pore-scale biofilm model and comparison with an experiment in a micro-fluidic flow cell. *Water Resour. Res.*, **2013**, 49(12), 8370-8382.

(20) Muyzer, G.; Stams, A. J. M. The ecology and biotechnology of sulphate-reducing bacteria. *Nat. Rev. Microbiol.*, **2008**, 6, 441-454.

(21) Laitinen, R. S. Selenium sulfide ring molecules. *Acta. Chem. Scand.*, **1987**, A41, 361-376.

(22) Rittmann, B. E.; McCarty, P. L. *Environmental Biotechnology: Principles and Applications*; McGraw-Hill Companies, Inc.: New York, U.S.A., 2001.

(23) Minaev, V. S.; Timoshenkov, S. P.; Kalugin, V. V. Structural and phase transformations in condensed selenium. *J. Optoelectron. Adv. M.*, **2005**, 7(4), 1717-1741.

(24) Robie, R. A.; Hemingway, B. S.; Fisher, J. R. *Thermodynamic Properties of Minerals and Related Substances at 298.15 K and 1 Bar (105 Pascals) Pressure and at Higher Temperatures*; United States Government Printing Office: Washington, U.S.A., 1978.

(25) Agency for Toxic Substances & Disease Registry; http://www.atsdr.cdc.gov/spl/

(26) World Health Organization; http://www.who.int/water_sanitation_health/dwq/chemicals/selenium.pdf

(27) Nambi, I. M.; Werth, C. J.; Sanford, R. A.; Valocchi, A. J. Pore-scale analysis of anaerobic halorespiring bacterial growth along the transverse mixing zone of an etched silicon pore network, *Environ. Sci. Technol.* **2003**, 37 (24), 5617-24.

(28) Maillacheruvu, K. Y.; Parkin, G. F. Kinetics of growth, substrate utilization and sulfide toxicity for propionate, acetate, and hydrogen utilizers in anaerobic systems. *Water Environ. Res.*, **1996**, 68(7), 1099-1106.

(29) Gharieb, M. M.; Gadd, G. M. The kinetics of ^{75}[Se]-selenite uptake by *Saccharomyces cerevisiae* and the vacuolization response to high concentrations. *Mycol. Res.*, **2004**, 108(12), 1415-1422.

(30) Tang, Y.; Ontiveros-Valencia, A.; Feng, L.; Zhou, C.; Krajmalnik-Brown, R.; Rittmann, B. E. A biofilm model to understand the onset of sulfate reduction in denitrifying membrane biofilm reactors. *Biotechnol. Bioeng.*, **2013**, 110(3), 763-772.

(31) Acharya, R. C.; Valocchi, A. J.; Werth, C. J.; Willingham, T. W. Pore-scale simulation of dispersion and reaction along a transverse mixing zone in two-dimensional porous media, *Water Resour. Res.* **2007**, 43, W10435, doi:10.1029/2007WR005969.

(32) Delgado, J. M. P. Q. Longitudinal and transverse dispersion in porous media._*Chem. Eng. Res. Des.* **2007**, 85(A9), 1245-1252.

(33) U.S. EPA Contaminated Site Cleanup Information; http://cluin.org/products/newsltrs/tnandt/view.cfm?issue=0108.cfm

(34) Kessi, J. Enzymic systems proposed to be involved in the dissimilatory reduction of selenite in the purple non-sulfur bacteria *Rhodospirillum rubrum* and *Rhodobacter capsulatus*, *Microbiology* **2006**, 152, 731-743.

(35) Losi, M. E.; Frankenberger, W. T. Jr. Bioremediation of selenium in soil and water, *Soil Sci.* **1997**, 162(10), 692-702.

(36) Chomsurin, C.; Werth, C. J. Analysis of pore-scale nonaqueous phase liquid dissolution in etched silicon pore networks, *Water Resour. Res.* **2003**, 39(9); DOI 10.1029/2002WR001643.

Table 1 Model Inputs[b]

Symbols	Description (Units)	Values and References
K_i	Half-maximum-rate concentration of dissolved chemical species *i* (mol/m^3)	K_1 = 0.37[28] K_2 = 0.054[29] K_3 = 0.02[30] K_5 = 0.78[28]
$k_{max,i,j}$	Maximum specific utilization rate of dissolved chemical species *i* in reaction *j* (mol/mol $C_5H_7O_2N$-d)	$k_{max,1,1}$ = 3.3[28] $k_{max,1,3}$ = 3.3[28] $k_{max,2,3}$ = 5.0[28] $k_{max,2,4}$ = 16[28] $k_{max,3,1}$ = 2.5[28] $k_{max,3,2}$ = 8.1[28] $k_{max,5,2}$ = 8.1[28] $k_{max,5,4}$ = 8.1[28]
k_{SeS}	Reaction coefficient for selenium sulfide production (m^3/mol-d)	0.0057
Y_j	Biomass yield in reaction *j* (mol $C_5H_7O_2N$/mol electron donor)	Y_1 = 0.032[28] Y_2 = 0.013[28] Y_3 = 0.05[22] Y_4 = 0.02[22]
b	Decay coefficient of biomass (1/d)	0.02[28]
X	Biomass density (mol/m^3)	354[22]
D_T	Transverse dispersion coefficient of dissolved chemical species (m^2/d))	0.0005[a]
ϕ	Porosity of the porous media	0.39
U	Flow velocity at the inlets (m/d)	8.4

$C_{in,i}$	Concentration of chemical species *i* in the influent (mol/m^3)	$C_{in,1}$ = 10 $C_{in,2}$ = 5 $C_{in,3}$ = 0.1

Notes:

a) The transverse dispersion coefficient mainly depends on the Pèclet number (*Pe*): $P_e = \frac{Ul}{D_i}$ (*l* is the characteristic length of the pore, 300 μm), and it is estimated using the data in Acharya et al.[31] and Delgado[32].

b) We use subscripts *i* (1-5) and *j* (1-5) to denote the dissolved chemical species and reactions, respectively.

Table 2 Model Outputs

Symbols	Description	Units
$C_{D,i}$	Concentration of dissolved chemical species *i*	mol/m^3
$C_{X,n}$	Concentration of biomass species *n*	mol $C_5H_7O_2N$/m^3
$C_{S,m}$	Concentration of solid chemical species *m*	mol/m^3
$k_{D,i}$	Overall reaction rate of dissolved chemical species *i*	mol/m^3-d
$k_{X,n}$	Overall reaction rate of biomass species *n*	mol/m^3-d
$k_{S,m}$	Overall reaction rate of solid chemical species *m*	mol/m^3-d

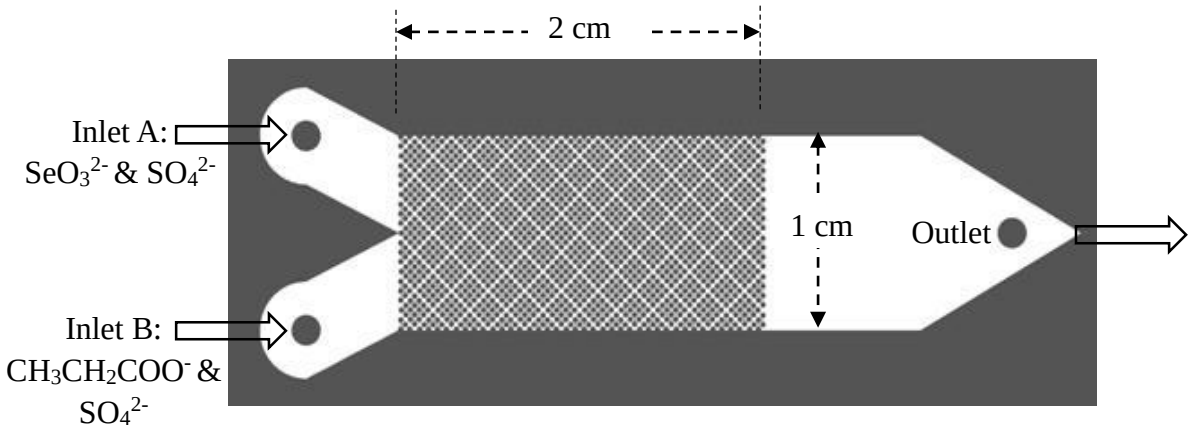

a)

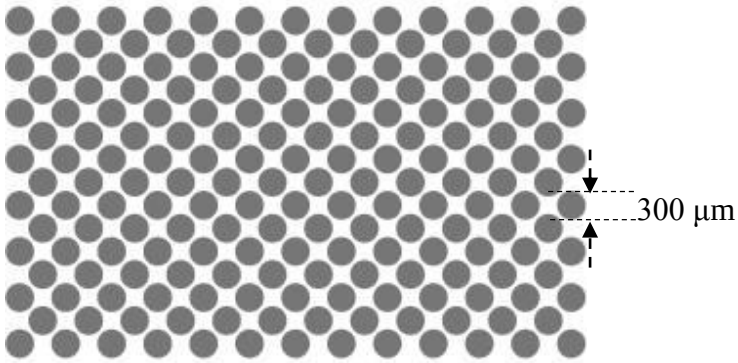

b)

Figure 1. Flow set-up of the micro-fluidic flow cell experiment (a) and homogeneous pore network in the flow cell.

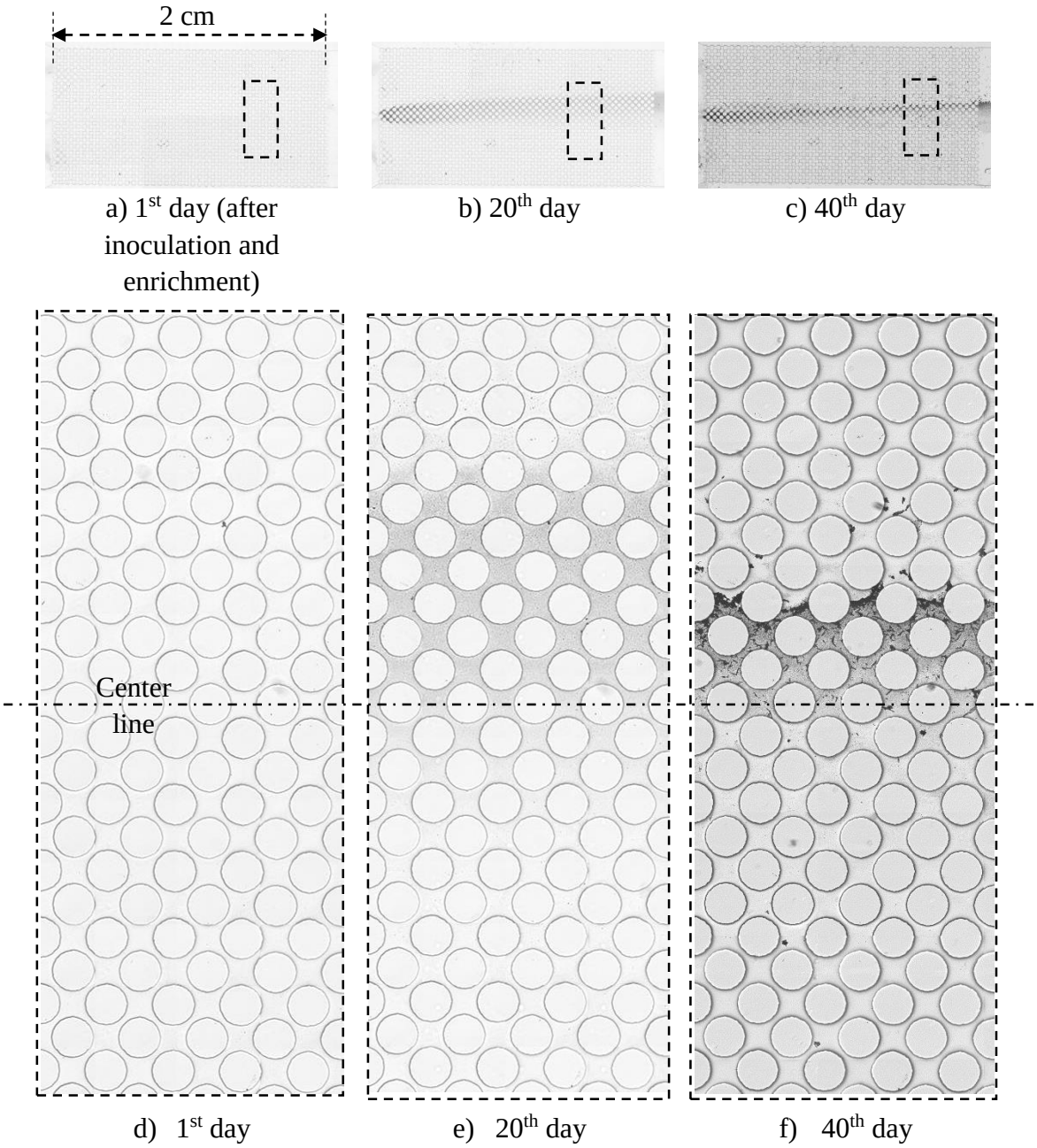

Figure 2. Reaction products in the flow cell at different time points of operation. The areas enclosed by rectangles in panels a), b) and c) are zoomed in in panels d), e) and f) respectively.

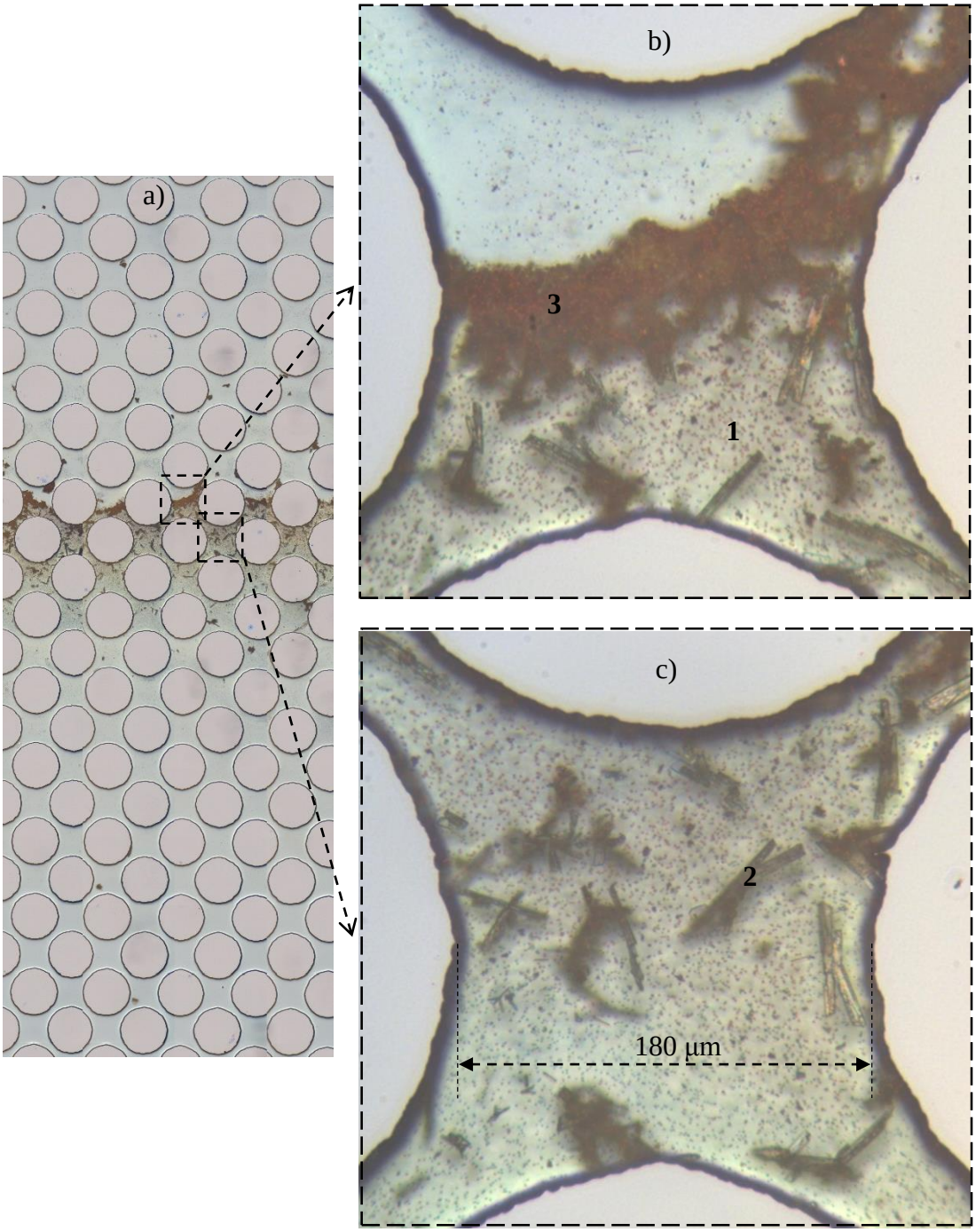

Figure 3. Distribution of reaction products on the 40th day of flow cell operation. a) Color image of the pore area from Figure 2f; b) Representative reaction products on the selenite-rich side of the mixing zone, dominated by red particles; c) Representative reaction products on the propionate-rich side of the mixing zone, dominated by long crystals.

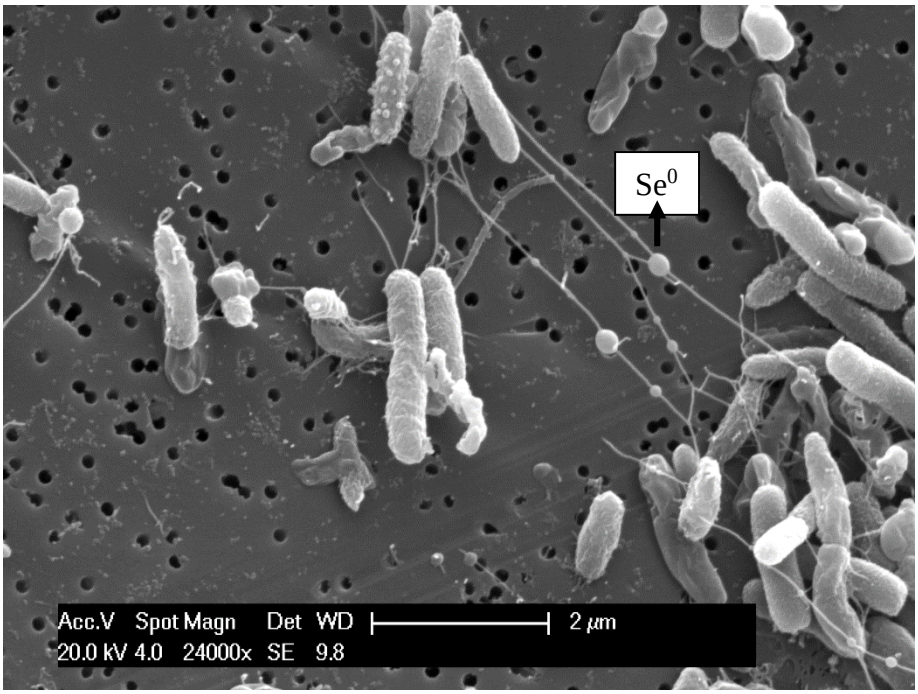

a) Elemental selenium particles attached to bacterial appendages

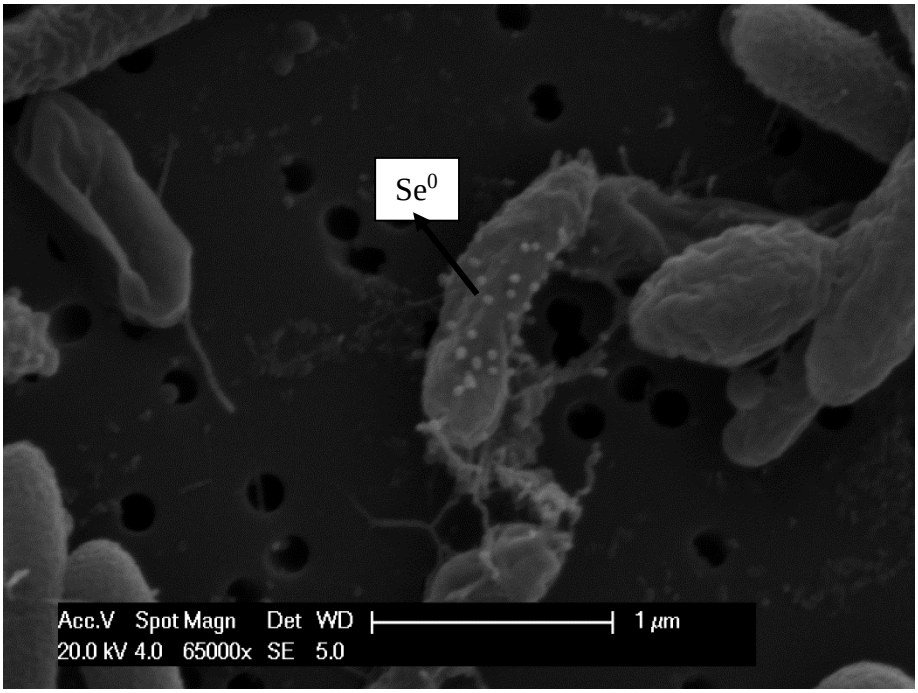

b) Elemental selenium particles attached to bacterial surface

Figure 4. Bacteria and elemental selenium particles at the flow-cell effluent. The effluent was filtered by membrane and the retentate on the membrane was then imaged using ESEM.

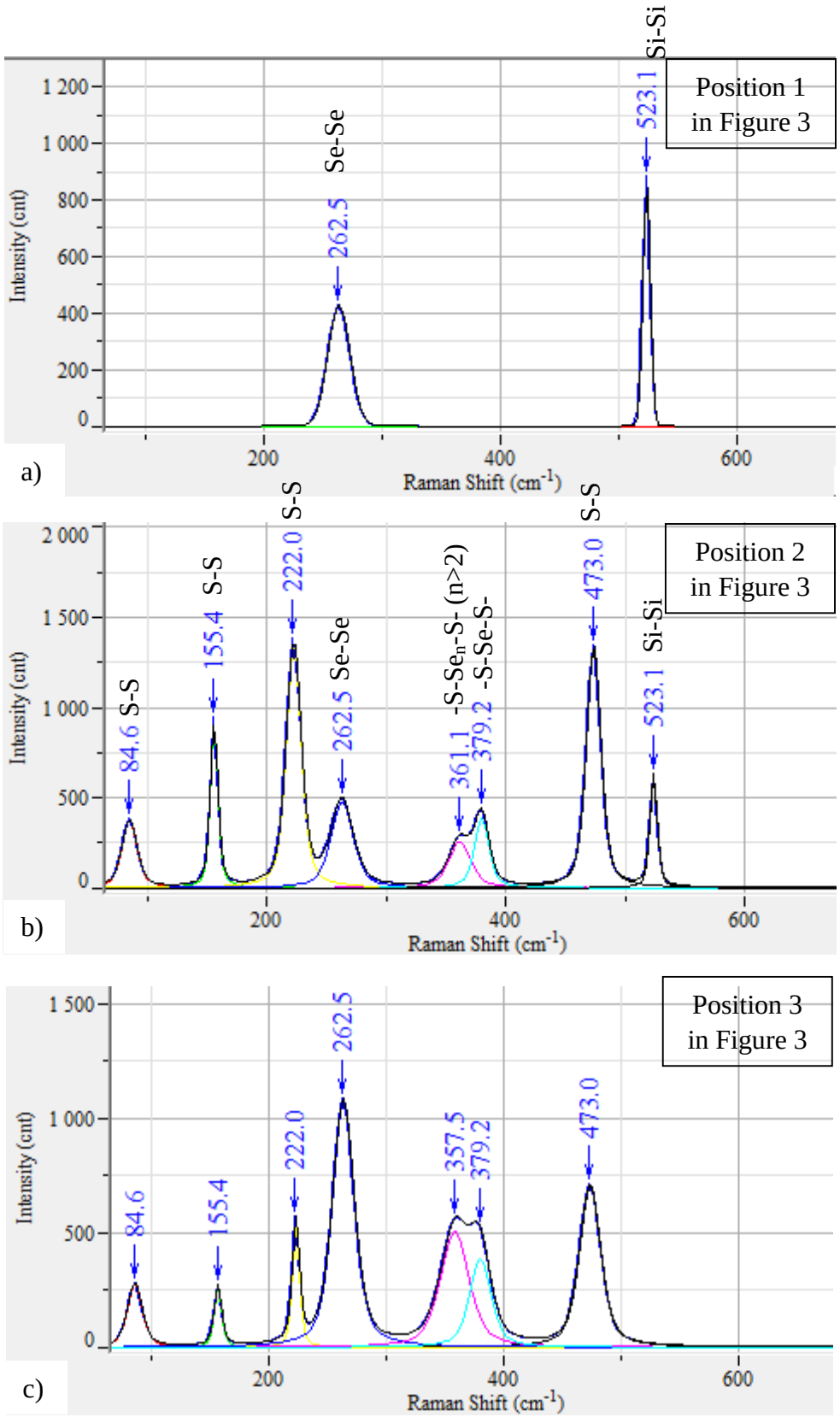

Figure 5. Raman spectra of the reaction products corresponding to positions 1 (a), 2 (b), and 3 (c) in Figure 3. The spectra are generated after baseline deduction and smoothing.

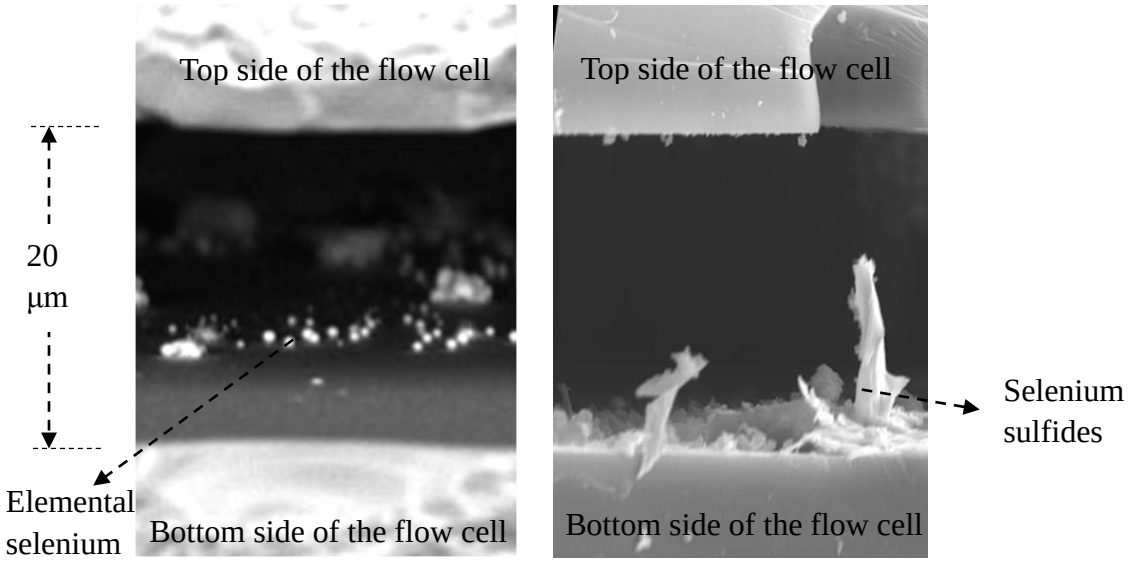

a) elemental selenium b) selenium sulfides

Figure 6. Representative ESEM images of pore cross-sections showing reaction products in the pore space. The composition of the products was obtained from EDS, as shown in Figure S2.

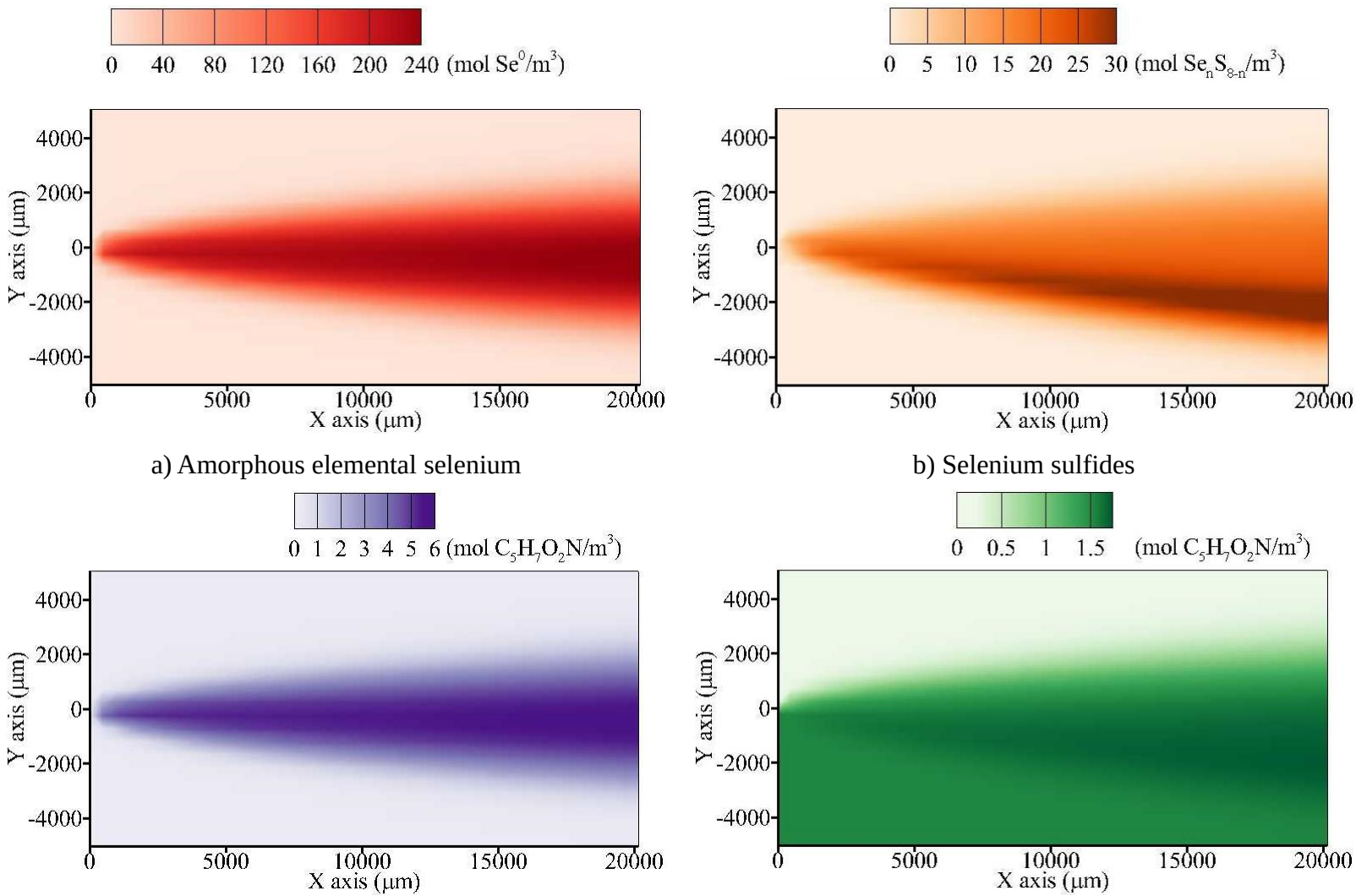

a) Amorphous elemental selenium

b) Selenium sulfides

c) Selenite-reducing bacteria

d) Sulfate-reducing bacteria

Figure 7. Simulated distribution of solid reaction products on the 40th day. The two types of selenium precipitates were spatially segregated (a, b) and the two bacterial species were also spatially segregated (c, d).